ACADEMIC PRESS

Available online at www.sciencedirect.com

SCIENCE DIRECT®

Journal of Magnetic Resonance 162 (2003) 380–384

JMR Journal of Magnetic Resonance

www.elsevier.com/locate/jmr

Measurement of spin–lattice relaxation times in EPR with enhanced orientation selectivity

Rüdiger-A. Eichel,* Josef Granwehr, and Arthur Schweiger

Physical Chemistry, ETH Zürich, CH-8093 Zurich, Switzerland

Received 22 October 2002; revised 6 March 2003

Abstract

Two schemes for the measurement of orientation-dependent spin–lattice relaxation times are introduced, which combine the inversion-recovery experiment with electron-Zeeman-resolved or right-angle wiggling EPR. The principles of the experiments are outlined and their performance is illustrated by examples of application. With the electron Zeeman-resolved approach the relaxation times of two metal complexes with different g values are unraveled, whereas with right-angle wiggling the orientation-dependent relaxation behavior of a metal complex with large hyperfine anisotropy is analyzed.

1. Introduction

For the measurement of relaxation times pulse EPR techniques are in general superior to continuous wave (cw) EPR. Two pulse EPR schemes are commonly used to measure spin–lattice relaxation times T_1. In the saturation-recovery (SR) EPR experiment a long mw pulse that saturates the electron spin transitions, is followed by a probe pulse or a spin-echo sequence to detect the recovery of the polarization [1,2]. In the inversion-recovery (IR) EPR experiment, a strong and short π pulse inverts the polarization [3]. In IR-EPR and SR-EPR experiments which are based on longitudinal detection [4], T_1 values as short as 20 ns could be measured [5]. This allows for the determination of spin–lattice relaxation times for metal complexes even at non-cryogenic temperatures, which is usually not possible by detecting the transverse magnetization because of short phase-memory times T_m.

All methods for the measurement of spin–lattice relaxation times are hampered by spectral diffusion. IR-EPR is usually more affected by spectral diffusion than SR-EPR [6], since population inversion is experimentally only achievable for a limited frequency range, determined by the selectivity of the inverting π pulse.

Moreover, relaxation times are often orientation-dependent. For the phase-memory time T_m typically a faster relaxation is observed for orientations of the paramagnetic species for which the resonance condition is more sensitive to a change in orientation [7,8]. As possible sources of the orientational dependence of T_1 the modulation of anisotropic hyperfine interactions [9] or the g anisotropy have been identified [10].

A critical item is the analysis of multi-exponential relaxation curves often observed in such studies. Least-square minimization algorithms provide good fits for a few exponentials whose number is known in advance. However, they tend to fail when the number of components becomes too large or is unknown. They also fail when the signal-to-noise ratio is poor, or if one of the relaxation components is a distribution of different relaxation times. Such an analysis might be ambiguous already for systems with two components. A more powerful method for the determination of the distributions of relaxation times or for multi-exponential relaxation curves is to invert the decay data and to get a quasi-continuous distribution of relaxation times [11]. Since this is usually an ill-posed problem, further assumptions about the data are required.

In this paper a new approach to enhance the orientation selectivity of IR-EPR experiments is described, using either an electron-Zeeman (EZ) resolved [12–14] or a right-angle wiggling (RAW) EPR [12,15,16] detec-

* Corresponding author.
E-mail address: eichel@phys.chem.ethz.ch (R.-A. Eichel).

1090-7807/03/$ - see front matter © 2003 Elsevier Science (USA). All rights reserved.
doi:10.1016/S1090-7807(03)00114-9

tion sequence. The experiments allow for a disentangling of EPR spectra into a second dimension which in the case of EZ-EPR represents the g value and in the case of RAW-EPR the orientation dependence. The inner working of the two experiments is described and their performance is demonstrated by two examples of application.

2. Electron-Zeeman resolved inversion-recovery experiment

In the EZ-IR EPR experiment, illustrated in Fig. 1a, the equilibrium polarization M_0 is inverted by a π pulse. After free evolution of variable time t_s the recovered polarization $M_z(t_s)$ is recorded with an EZ-EPR scheme, which consists of a primary echo sequence ($\pi/2$–τ–π–τ–echo) combined with a sinusoidal modulation of B_0 [13]. All pulses are assumed to be non-selective.

The motion of the magnetization vectors in the rotating frame for two spin systems k and l with $S = \frac{1}{2}$ and g values $g_k \neq g_l$ is illustrated in Fig. 1b. At Boltzmann equilibrium (time t_0), the two magnetization vectors are oriented along $\mathbf{B}_0 \| z$. After the π pulse (time t_1), the recovery of the longitudinal component of each of the two magnetization vectors can be described by [17]

$$M_z(t_s) = M_0\left[1 - 2\exp\left(-\frac{t_s}{T_1}\right)\right]. \tag{1}$$

Time t_s is incremented in steps of Δt and the experiment is repeated for N values $t_s = k\Delta t$, $1 \leqslant k \leqslant N$.

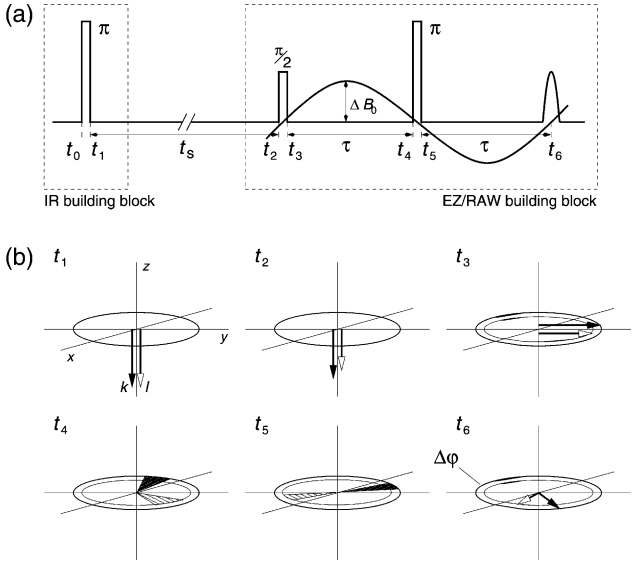

Fig. 1. (a) Timing diagram for the EZ-IR EPR and RAW-IR EPR experiments, consisting of a preparation π pulse followed by an EZ-EPR or RAW-EPR detection sequence with a sinusoidal field modulation. (b) Position of the magnetization vectors in the rotating frame for two species k (full arrows) and l (open arrows) with different g values, corresponding to the points in time indicated in (a).

The $\pi/2$ pulse along x creates transverse magnetization which is proportional to $M_z(t_s)$. It dephases during the free evolution period of time $\tau = t_4 - t_3$ and refocuses during the evolution period of time $\tau = t_6 - t_5$. Due to the B_0-field modulation, $B_m(t) = \Delta B_0 \sin(2\pi\nu_{ez}t)$, with amplitude ΔB_0 and frequency $\nu_{ez} = (2\tau)^{-1}$ the spins precess in the transverse plane with their g-value specific Larmor frequencies. Thus, magnetization vectors with different g values accumulate different phases, leading at time of echo formation to [13]

$$M(t_6) = -M_y\cos(\varphi_{ez}) - M_x\sin(\varphi_{ez}). \tag{2}$$

The phase

$$\varphi_{ez} = \frac{8g\beta_e}{h}\Delta B_0\tau \tag{3}$$

is proportional to ΔB_0 and the corresponding g value. The different phases cause the spin echo along the y-axis to oscillate as a function of ΔB_0.

The LC circuit used for the generation of the modulation field has a rise time of several microseconds. With a typical modulation frequency of $\nu_{ez} = 500\,\text{kHz}$, the magnetization recovers during 6–8 μs under an oscillating external field before the EZ-EPR sequence can be applied. Since the integral field change is small, the magnetization is virtually not affected by the modulation during time t_s.

Time Δt should be as short as possible, so that in the initial experiment with $k = 1$ ($t_s = \Delta t$), $M_z(t_s) \approx -M_0$. If the ΔB_0 modulation has to be started before the π pulse is applied, the time increments Δt have to be an integer multiple of ν_{ez}^{-1}. The π pulse is then applied at a zero-crossing of the field modulation and, neglecting pulse lengths,

$$\Delta t = 2k\tau = k\nu_{ez}^{-1}. \tag{4}$$

However, this procedure limits the measurement of spin–lattice relaxation times to values $T_1 > \Delta t$. For $T_1 \gg \nu_{ez}^{-1}$, the field modulation can be started *after* the π pulse and Eq. (4) has not to be fulfilled. This adds additional flexibility to the method since shorter Δt values can be used, leading to an improved accuracy of the data. It is then also possible to use long saturation pulses or more complex preparation sequences to enhance the selectivity of the method.

3. Right-angle wiggling inversion-recovery experiment

Consider a disordered spin system with an orientation-dependent spin–lattice relaxation time. Since the IR-EPR curves are recorded at a fixed B_0 field, a particular set of orientations is selected. Typically, for rhombic systems, only the extreme low- and high-field settings, and for axial systems only the setting ($\mathbf{B}_0 \| g_\parallel$) provide an orientation selectivity where a single orien-

tation contributes to the spectrum. At intermediate field settings many different orientations are simultaneously excited. The orientation selectivity can be improved with an RAW-EPR experiment which is based on a rapid change of the relative orientation between $\mathbf{B}_0$ and the sample during a primary or a stimulated echo sequence [15,16]. This results in a shift of the resonance frequencies that is characteristic for each orientation. In the RAW-EPR spectrum, resonances from different orientations are unraveled in a new dimension, which is proportional to the gradient of the change in resonance frequency. Experimentally, the reorientation is performed by applying a sinusoidal field modulation *perpendicular* to $\mathbf{B}_0$. The timing diagram is the same as used for the EZ-IR experiment.

The description of the RAW-IR EPR experiment for an $S = \frac{1}{2}$ model system differs from the EZ-IR EPR experiment only in the effect of the detector sequence. During the two-pulse echo sequence, the magnetizations precess in the transverse plane with their orientation-specific Larmor frequencies. Thus, magnetization vectors corresponding to different orientations accumulate different phase angles, leading at time of echo formation to [16]

$$M(t_6) = -M_y \cos(\varphi_{\mathrm{raw}}) - M_x \sin(\varphi_{\mathrm{raw}}) \tag{5}$$

with an RAW phase φ_{raw} proportional to ΔB_0 and the corresponding orientation.

4. Experimental

All experiments were carried out at 15 K on a home-built X-band pulse EPR spectrometer [18] equipped with a home-built dielectric ring resonator [19]. Pulse lengths of $t_{\mathrm{p}} = 20$ ns for both the $\pi/2$ and π pulses, a fixed interpulse spacing τ of 980 ns, and modulation frequencies of $\nu_{\mathrm{ez}} = \nu_{\mathrm{raw}} = 500$ kHz were used. For the measurement of T_1 by an inversion-recovery experiment, the bandwidth of the preparation π pulse has to be much larger than the bandwidth of the detection sequence, which was achieved by integrating over the whole echo signal. As in the conventional IR-EPR experiment, a two-step phase cycle $[(\pi) + (-\pi)]$ of the preparation π pulse was used and relaxation curves recorded with ΔB_0 and $-\Delta B_0$ were added. Dependent upon the T_1 relaxation times that limit the repetition time of the experiment, a typical 2D experiment at a particular B_0-field setting lasted approximately 5 h.

The recovery of the magnetization was recorded in 600 steps, starting at $t_s = \Delta t = 2\,\mu$s. In all experiments ΔB_0 was varied from 0 to 15 mT in steps of 0.3 mT. In the data analysis, first, the EZ or RAW dimension of the spectrum was obtained by Fourier transformation of the data with respect to ΔB_0. Then, slices at fixed g values in the EZ dimension or fixed gradients in the RAW dimension were taken containing the relaxation transients for distinct orientations. The relaxation curves were then analyzed with a nonlinear least-square fit using a Marquardt–Newton–Gauss algorithm [20]. The reference equation to which the experimental relaxation curves were fitted was of the form

$$S(t_s) = \sum_{i=1}^{n} A_i \left[1 - k_i \exp\left(-\left(\frac{t_s}{T_{1,i}} \right)^{\alpha_i} \right) \right], \tag{6}$$

where A_i is the amplitude of component i, k_i represents the efficiency of the inversion process, $T_{1,i}$ is the relaxation time, and α_i is a parameter accounting for a distribution of $T_{1,i}$ that leads to a stretched exponential. If $T_{1,i}$ is a single exponential, $\alpha_i = 1$, and in case of a distribution of $T_{1,i}$, $\alpha_i < 1$. The analysis depends on the distribution of $T_{1,i}$ [21]. The number n of components to be fitted had to be preset. The optimum value for IR-EPR is $k_i = 2$ which is usually not fully attained.

To allow for a stable fit the number of parameters should be kept as small as possible. In Eq. (6) this number can be reduced by subtracting the signal amplitude $S_0 = \sum_i A_i$, corresponding to an infinite evolution time t_s. The formula is then given by

$$S(t_s) - S_0 = -\sum_{i=1}^{n} b_i \exp\left(-\left(\frac{t_s}{T_{1,i}} \right)^{\alpha_i} \right), \tag{7}$$

with $b_i = A_i k_i$. To get a more stable fit for noisy measurements, unwanted signals on a time scale short compared to T_1 can be reduced by calculating a moving average over a few data points [5].

T_1 usually describes the mono-exponential decay of a particular spin species. For a better readability of the formulae, we use T_1 in Eqs. (6) and (7) without this explicit restriction, thus i runs over all exponential and stretched-exponential relaxation components of all spin species. For a multi-exponential decay, the time constants are denoted by T_1', T_1'', etc.

5. Results

5.1. EZ-IR EPR

As an example for the EZ-IR EPR experiment the spin–lattice relaxation times of a mixture of bis(salicylaldoximato)Cu(II), $Cu(sal)_2$, diluted in $Ni(sal)_2$ powder, with $g_\perp = 2.04 \leqslant g \leqslant g_\parallel = 2.19$ [22,23] and of vanadylpyrophosphate, $VO(IV)(P_2O_7)_2$, in $Zn(P_2O_7)_2$ powder with $g_\parallel = 1.93 \leqslant g \leqslant g_\perp = 1.98$ [24] are separated at $B_0 = 320$ mT, where the EPR spectra of the two compounds overlap due to large hyperfine splittings (arrow in Fig. 2a). In the EZ-EPR experiment, the two spectra are fully separated (Fig. 2b). Fig. 2c shows the relaxation curves of a conventional IR-EPR experiment, to which both species contribute. In Figs. 2d and e relax-

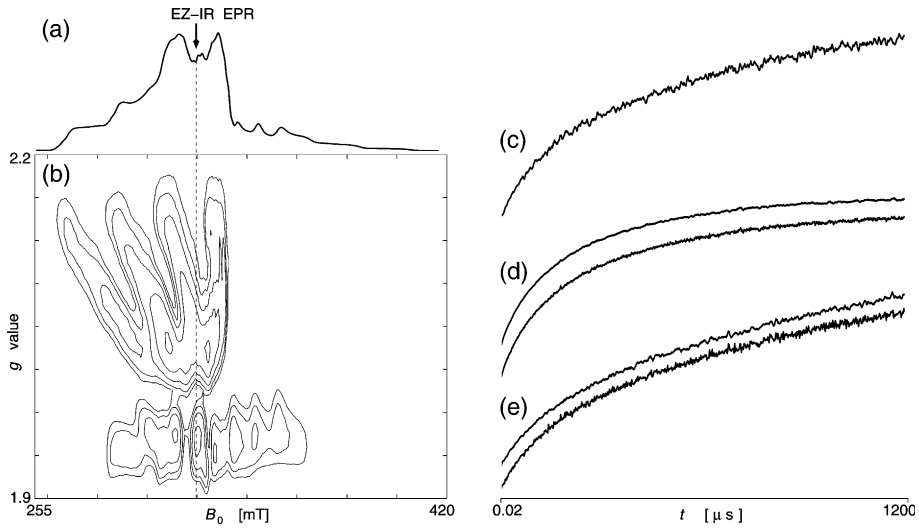

Fig. 2. Powder EPR measurements of a sample consisting of a mixture of $Cu(sal)_2$ and $VO(P_2O_7)_2$, $\nu_{mw} = 9.148$ GHz. The relaxation curves were taken at $B_0 = 320$ mT. (a) Echo-detected EPR spectrum. (b) EZ-EPR spectrum. (c) IR-EPR experiment on a mixture of $Cu(sal)_2$ and $VO(P_2O_7)_2$. (d) Relaxation curves of $Cu(sal)_2$, IR-EPR experiment of a sample which only contains $Cu(sal)_2$ (top), EZ-IR EPR experiment of the mixture (bottom). (e) Relaxation curves of $VO(P_2O_7)_2$, IR-EPR experiment of a sample which only contains $VO(P_2O_7)_2$ (top), EZ-IR EPR experiment of the mixture (bottom).

ation curves for $Cu(sal)_2$ and $VO(P_2O_7)_2$ (bottom) separated in the EZ-EPR experiment are compared with the standard IR-EPR relaxation measurements of the individual samples which either contain pure $Cu(sal)_2$ or $VO(P_2O_7)_2$ only (top). The relaxation transients could nicely be fitted by assuming a biexponential. The relaxation times obtained with the different techniques are collected in Table 1.

Table 1
Spin–lattice relaxation times (in μs) for a sample consisting of bis(salicylaldoximato)Cu(II), $Cu(sal)_2$, diluted in $Ni(sal)_2$ powder, and of vanadyl-pyrophosphate, $VO(IV)(P_2O_7)_2$, in $Zn(P_2O_7)_2$ powder

Method	$VO(P_2O_7)_2$		$Cu(sal)_2$	
	T_1'	T_1''	T_1'	T_1''
EZ-IR EPR	108 ± 5	994 ± 50	90 ± 5	421 ± 20
IR-EPR	130 ± 5	1258 ± 50	84 ± 5	359 ± 10

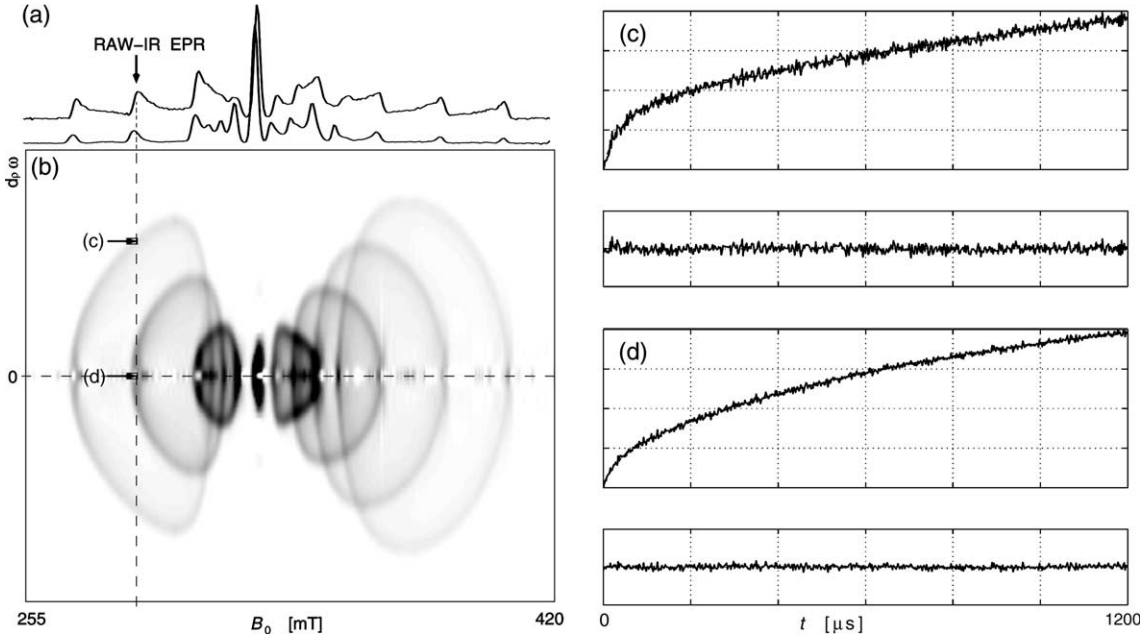

Fig. 3. EPR measurements of $VO(P_2O_7)_2$, $\nu_{mw} = 9.148$ GHz. (a) Powder EPR spectrum (top) and slice of the RAW-EPR spectrum along the canonical orientations (bottom). (b) RAW-EPR spectrum. (c,d) RAW-IR EPR-separated relaxation curves for an intermediate orientation of the $m_I = -\frac{7}{2}$ manifold (c) and the parallel orientation of the $m_I = -\frac{5}{2}$ manifold (d). Doubly exponential fits (dashed lines) (top) with the corresponding residuals (bottom).

5.2. RAW-IR EPR

The versatility of RAW-IR EPR is illustrated on $VO(IV)(P_2O_7)_2$ in $Zn(P_2O_7)_2$. The experimental EPR and RAW-EPR spectra are shown in Figs. 3a and b. At $B_0 = 290\,\mathrm{mT}$ (indicated by an arrow) the parallel orientation of the $m_I = -\frac{5}{2}$ manifold overlaps with noncanonical orientations of the $m_I = -\frac{7}{2}$ manifold. In general, T_1 is faster at an intermediate orientation, than along a canonical orientation [10].

The RAW-IR EPR relaxation curves for the two m_I manifolds, shown in Fig. 3c and d, can nicely be fitted by assuming one exponential and one stretched exponential. The faster relaxation times with $T'_{1,\mathrm{int}} = 38 \pm 2\,\mu\mathrm{s}$ for the intermediate orientation ($m_I = -7/2$) and $T'_{1,\parallel} = 43 \pm 2\,\mu\mathrm{s}$ for the parallel orientation ($m_I = -5/2$) vary only little between the two orientations, whereas the slower relaxing components T''_1 show a considerable orientation dependence. As expected, the relaxation time for the intermediate orientation, $T''_{1,\mathrm{int}} = 808 \pm 40\,\mu\mathrm{s}$, is faster than the one for the parallel orientation, $T''_{1,\parallel} = 1321 \pm 50\,\mu\mathrm{s}$.

6. Conclusion and outlook

EZ-IR EPR and RAW-IR EPR are extensions of the conventional IR-EPR technique to measure spin–lattice relaxation times. EZ-IR EPR allows the separation of overlapping components with different g values, whereas RAW-IR EPR provides enhanced orientation selectivity for disentangling relaxation curves of disordered systems. In samples which contain only one type of paramagnetic species the relaxation times obtained with the new experiments and with the conventional IR-EPR experiment are the same.

In EZ-IR EPR the inverting π pulse is applied at a zero-crossing of the field modulation. To study spectral diffusion processes, the π pulse could also be applied at B_0, while detection is done at $B_0 + \Delta B_0$. This would offer an alternative to pulse ELDOR [25].

Acknowledgments

We thank Jeffrey Harmer for the Matlab routine to fit the data and Walter Lämmler for the sample preparation. This research has been supported by the Swiss National Science Foundation.

References

[1] N. Bloembergen, S. Wang, Phys. Rev. 93 (1954) 72.
[2] S.I. Weissmann, G. Feher, E.A. Gere, J. Am. Chem. Soc. 79 (1957) 5584.
[3] J.R. Norris, M.C. Thurnauer, M.K. Bowman, Adv. Biol. Med. Phys. 17 (1980) 365.
[4] J. Granwehr, A. Schweiger, J. Magn. Reson. 151 (2001) 78.
[5] J. Granwehr, A. Schweiger, Appl. Magn. Reson. 20 (2001) 137.
[6] W.F. Beck, J.B. Innes, J.B. Lynch, G.W. Brudvig, J. Magn. Reson. 91 (1991) 12.
[7] A.H. Beth, B.H. Robinson, Biol. Magn. Reson. 8 (1989) 179.
[8] J.L. Du, K.M. More, S.S. Eaton, G.R. Eaton, Isr. J. Chem. 32 (1992) 351.
[9] I.V. Aleksandrov, G.M. Zhidomirov, J. Exp. Theor. Phys. (USSR) 41 (1961) 127.
[10] J.L. Du, G.R. Eaton, S.S. Eaton, J. Magn. Reson. 115 (1995) 213–221; J. Magn. Reson. 115 (1995) 236; J. Magn. Reson. 117 (1995) 67.
[11] G.C. Borgia, R.J.S. Brown, P. Fantazzini, J. Magn. Reson. 132 (1998) 65.
[12] R.-A. Eichel, Ph.D. thesis, ETH Zürich, No. 14394, 2001.
[13] R.-A. Eichel, A. Schweiger, J. Magn. Reson. 152 (2001) 276.
[14] R.-A. Eichel, A. Schweiger, Chem. Phys. Lett. 358 (2002) 271.
[15] R.-A. Eichel, A. Schweiger, J. Chem. Phys. 115 (2001) 9126.
[16] R.-A. Eichel, A. Schweiger, Mol. Phys. 100 (2002) 3661.
[17] R.R. Ernst, G. Bodenhausen, A. Wokaun, Principles of Nuclear Magnetic Resonance in One and Two Dimensions, Clarendon Press, Oxford, 1987.
[18] T. Wacker, Ph.D. thesis, ETH Zürich, No. 9913, 1992.
[19] G.A. Sierra, Ph.D. thesis, ETH Zürich, No. 12241, 1997.
[20] W.H. Press, S.A. Teukolsky, W.T. Vetterling, B.P. Flannery, Numerical Recipes in C, second ed., Cambridge University Press, Cambridge, 1992.
[21] P. Borgs, K.W. Kehr, P. Heitjans, Phys. Rev. B 52 (1995) 6668.
[22] A. Schweiger, G. Rist, H.H. Günthard, Chem. Phys. Lett. 31 (1975) 48.
[23] A. Schweiger, H.H. Günthard, Chem. Phys. 32 (1978) 36.
[24] H. van Willigen, J. Magn. Reson. 39 (1980) 37.
[25] A. Schweiger, G. Jeschke, Principles of Pulse Electron Paramagnetic Resonance, Oxford University Press, Oxford, 2001.